The University of Tehran Press

Pollution

Print ISSN: 2383-451X
Online ISSN: 2383-4501

https://jpoll.ut.ac.ir/

Enhanced Removal of Chromate from Aqueous Solution Using a Metal Oxide Nanocomposite Derived from Bimetallic Metal Organic Framework with Both Adsorption and Catalytic Properties

Hadi Salari[1]✉ | **Ali Zeraatkar Moghaddam**[2]✉

1. Department of Chemistry, College of Sciences, Shiraz University, Shiraz, Iran.
2. Department of Chemistry, Faculty of Science, University of Birjand, South Khorasan, Birjand, Iran.

Article Info

Article type:
Research Article

Article history:
Received: 3 June 2023
Revised: 12 September 2023
Accepted: 5 December 2023

Keywords:
Chromate removal
Synergism
Metal organic framework

ABSTRACT

Removing environmental pollutants and preserving the environment is an important issue and many efforts have been made in this regard in recent years. In the present work, chromate ions were removed from aqueous solutions by ZnO/CuO acting as both adsorbent and catalyst. Metal oxide fabrication from metal organic framework is one of the most important and interesting scientific issues for the synthesis of high surface area materials. Here, we demonstrate ZnO/CuO synthesis from bimetallic Zn-Cu metal-organic framework (Zn(50)-Cu(50)-BTC) using temperature-programmed oxidation method. The adsorptive and catalytic removal procedure were optimized in terms of its batch efficiency using experimental designs. The effect of hole scavenger type was investigated, and the relationships between the effective important removal procedure parameters and chromate removal efficiency were analyzed through the response surface methodology (RSM) based on central composite design (CCD). The correlation coefficient (R^2) and F values were 0.9883 and 74.81, respectively. Finally, simplex non-linear optimization was carried out and the optimal pH, ZnO/CuO amount and contact time were determined to be 2, 20 mg, and 17.5 min. Under these conditions, the predicted removal efficiency of 50 ppm chromate at a 95% confidence level was 98.1 ± 2.4%, which was very close to the recorded response (i.e. 99.4 ± 1.9%). The kinetic and isothermal profiles of the proposed ZnO/CuO, were thoroughly investigated under optimal conditions. The adsorption isotherm follow the Langmuir model and kinetics were found to be pseudo-second-order.

Cite this article: Salari, H., & Zeraatkar Moghaddam, A. (2024). Enhanced Removal of Chromate from Aqueous Solution Using a Metal Oxide Nanocomposite Derived from Bimetallic Metal Organic Framework with Both Adsorption and Catalytic Properties. *Pollution*, 10 (1), 134-150.
https://doi.org/10.22059/poll.2023.360286.1932

DOI: https://doi.org/10.22059/poll.2023.360286.1932

INTRODUCTION

These days, contamination of groundwater resources with different pollutants like sulfate, nitrate, pesticide and chromate ions, is a serious threat to the drinking water resources and hence a global problem (Li et al., 2016). The enduring presence of such contaminants in rivers, soil and ground waters, can lead to damaging effects like the changes in the structure of microbial communities (Olivares et al., 2010, Sołek-Podwika et al., 2016, Liu et al., 2015).

As an important pollutant, chromate ions originate come from electroplating, mining, tanning and the fertilizing industries. These toxic ions can cause harm to plant and animal lives, and has been known as a carcinogenic agent causing skin cancers or respiratory hypersensitivity due to direct exposure (Babiker et al., 2004, Ajmal et al., 1984, Saha et al., 2011). The highly mobile chromate anions can contaminate surface/ground waters and hence their elimination from the environment can lower the risks posed to people and ecosystems (Tzou et al., 1998).

*Corresponding Author Email: *hsalari@shirazu.ac.ir*
a_zeraatkar_m@birjand.ac.ir

Different methods, like chemical reduction, photocatalysis, coagulation, and lime softening, have been reportedly used to this end. Yet, they are known to be costly, and to produce harmful by-products in addition to being rather inefficient, especially at low chromate concentration (Wielinga et al., 2001, Golbaz et al., 2014, Sharma et al., 2008, Salari and Zahiri, 2022, Venkatesh et al., 2022).

Alternatively, adsorbent-based approaches could be interesting choices for this purpose and hence various studies have been performed on eliminating chromate ions from water samples using metal oxides, polymers, organic or inorganic hybrids or ion-exchanging materials (Salari et al., 2022, Barlik et al., 2016, Nalbandian et al., 2016).

Metal-organic frameworks (MOFs) have recently been produced due to their high surface area, persistent porosity, diverse topologies, and changeable functional groups formed via coordination connections of metal ions and organic ligands (Salari and Sadeghinia, 2019, Furukawa et al., 2013). These features provide MOFs with significant benefits in a wide range of applications, such as sensing, separating, catalytic, and electrochemical capacitors (Gao et al., 2019, Shayeh and Salari, 2020). These advantages stem from the tailorable porous architectures and various active sites that have proven MOFs to be suitable adsorbents and/or catalysts for water and wastewater treatment.

In recent years, scientific groups have examined the feasibility of converting MOF into supported metal oxide nanoparticles. In this scenario, MOF serves as an appropriate template for the production of metal oxide nanoparticles. For example, fabrication of *a*-Fe_2O_3 from MIL-88-Fe, and Co_3O_4 from ZIF-67 have been shown (Xu et al., 2012, Shao et al., 2014). Structures produced by this method have different physical and chemical properties than those that are synthesized by conventional methods. Co_3O_4 nanostructure which was derived from MOF, was applied in lithium-ion batteries, and $Co(OH)_2$ synthesized from a Cobalt based MOF was used in supercapacitors (Li et al., 2015, Wang et al., 2015b).

Based on what was said, the present research focused on synthesis, characterization and application of ZnO/CuO as metal oxide nanocomposite derived from bimetallic MOF in chromate removing from aqueous solutions. Here, the MOF structure plays precursor role in the synthesis of a structure with unique properties. The observations showed that the proposed metal oxide nanocomposite acting as both adsorbent and catalyst. The ZnO/CuO was investigated in removing of chromate under different conditions and the best operating conditions were also determined using the simplex non-linear optimization method. Isothermal and kinetic behavior of the ZnO/CuO were evaluated under the determined optimal conditions. The adsorbent was also used to remove chromate from water and wastewater specimens, and their regeneration and reuse potentials were studies.

MATERIALS AND METHODS

$Cu(NO_3)_2.3H_2O$ and $Zn(NO_3)_2.6H_2O$ used as copper and zinc sources, respectively. Benzene-1,3,5-tricarboxylic acid (H_3BTC) [Trimesic acid, Merck] was utilized as organic ligand for MOF synthesis. Potassium dichromate [$K_2Cr_2O_7$, Merck] and 1,5-diphenylcarbazide [Merck] used as pollutant and reagent, respectively. All additional chemicals were obtained from Merck Chemical Co. and utilized directly without further purification. Stock solutions were diluted with deionized (DI) water to create the solutions. Suitable concentrations of 0.1 M HCl or 0.1 M NaOH solutions were used to control the pH of the solutions.

1 g H_3BTC was dissolved in 30 mL DI water. By controlling the pH to 7, a clear solution was obtained. 0.5 g $Cu(NO_3)_2.3H_2O$ was placed in vessel A and by adding 20 mL DI water, the solid was dissolved. 0.7 g $Zn(NO_3)_2.6H_2O$ was dissolved in 20 mL DI water in vessel B. The contents of vessels A and B were added to Benzene-1,3,5-tricarboxylic acid solution drop by drop. To avoid Benzene-1,3,5-tricarboxylic acid and $Cu(OH)_2$ precipitation, the pH should be controlled

at around 7. The reaction was carried out for 12 hours at stirring rate of 800 rpm. The resulted Zn(50)-Cu(50)-BTC MOF was filtered and washed by water and ethanol respectively a number of times and sample was dried at 80 °C for 12 h (Salari and Sadeghinia, 2019).

Thermal decomposition of pristine MOF yielded ZnO/CuO, according to temperature program shown in figure 1 (Salari and Sadeghinia, 2019). Thermal oxidation of copper at temperature range of 300-550 °C produces CuO and at 200 °C, Cu_2O will be formed (Shaislamov et al., 2016). Very slow ramp rate was selected and final temperature was kept at 330 °C for 3h to prevent the sintering of Cu particles while simultaneously ensuring the production of crystalline CuO phase. Temperature quenching have been done slowly (2 °C/min) to intercept any stress to metal oxide structure. After pyrolysis, the black fine powder was obtained.

The sample's X-ray diffraction (XRD) pattern was recorded using a Philips X-ray diffractometer equipped with a Ni-filtered CuK_α radiation source (λ = 1.5418 Å) (2θ =10-70°). The specific surface area of prepared sample was measured by nitrogen adsorption–desorption according to the Brunauer-Emmet-Teller (BET) equation using Belsorp apparatus. Pore size distribution was computed based on Barret-Johner-Halenda (BJH) analysis. To do this analysis, metal oxide sample was degased at 200 °C fistly, and BET plot of ZnO/CuO collected in the pressure range of 0.05-1 and P/P_0=0.99.

Using a Perkin Elmer PE-1600-FTIR spectrophotometer, the Fourier transform infrared (FTIR) spectra of KBr pellets were acquired in the 4000-400 cm^{-1} region. The surface morphology and elemental analysis were explored using scanning electron microscope (SEM, KYKY3200

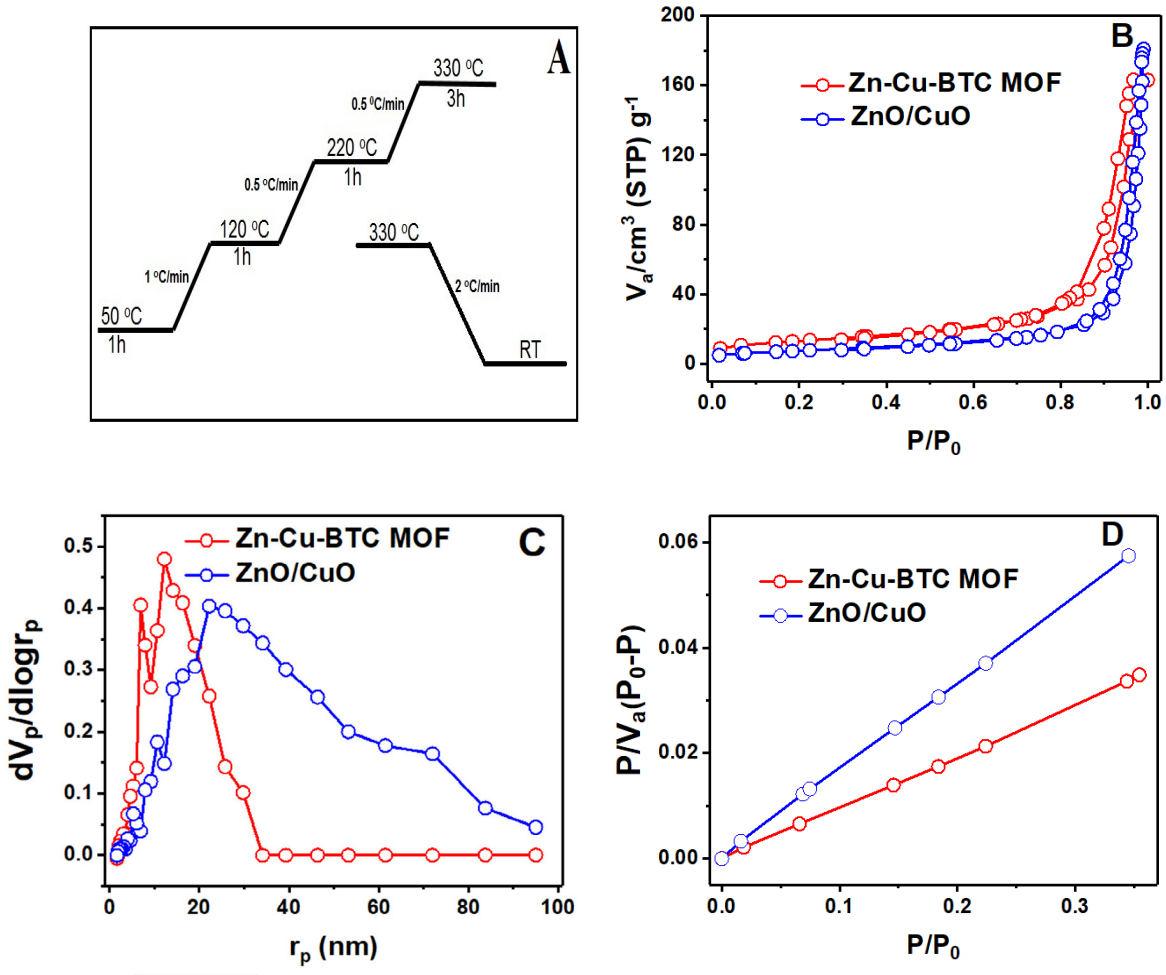

Fig. 1. Temperature program for oxidation of Zn(50)-Cu(50)-BTC MOF (A), Adsorption-desorption isotherm (B), BJH plots (C) and BET curves of Cu(50)-Zn(50)-BTC MOF and ZnO/CuO (D).

model) equipped with a Bruker energy dispersive X-Ray (EDX). X-ray photoelectron spectroscopy (XPS) was performed using a monochromatic Al K source and a Bestec Ultra spectrometer. To measure the amount of chromate in aqueous samples, an Analytikjena Specord 210 UV/Vis spectrophotometer was employed. A combination glass electrode and a SCHOTT pH-meter were used to take pH values.

The removal procedure was performed in a 50 mL glass cylindrical vessel with the temperature controlling. 10 mL of the chromate solution was brought into contact with a defined amount of the ZnO/CuO and hole scavenger at desired pH values and subjected to agitation for a definite period under a constant temperature regime until equilibrium was reached. Once equilibrium was established, the ZnO/CuO was separated, filtered and the chromate concentrations were determined using appropriate reagents through UV-Vis spectrophotometery analysis based on the reported literature (Shamshirgaran et al., 2022).

Using the difference between their starting (C_o) and final (C_e) concentrations in the solutions, the removal efficiency (%R) was computed:

$$\%R = \frac{(C_0 - C_e)}{C_0} \times 100 \quad (1)$$

RESULTS AND DISCUSSION

Characterization studies

The BET curves, BJH plots and adsorption/desorption isotherms of Zn-Cu-BTC MOF and ZnO/CuO are shown in Fig. 1. From the N_2-adsorption-desorption graphs, we can conclude that the surface area decreases and pore volume remains constant with the organic part coming out of the MOF structure (Salari and Sadeghinia, 2019). Porous structures of Zn-Cu-BTC MOF and ZnO/CuO with surface area of 46.6 and 26.6 m^2/gr and pore volume of 0.19 and 0.22 achieved respectively (Salari and Sadeghinia, 2019). After pyrolysis the mean diameter increased and pore volume remained constant. High surface area can facilitate the adsorption on catalysts surface.

The crystalline properties of Zn-Cu-BTC MOF and ZnO/CuO structures were investigated by X-ray diffraction techniques (Fig. 2A). The difference in peaks intensity in MOF relates to occlusion of pore due to presence of guest molecule (Shaislamov et al., 2016, Feldblyum et al., 2011). Copper and zinc have the same radius and because of the random distribution of metal ions in different molar ratios of copper and zinc at the same location in the framework and the homogeneity of electron density, there is no difference in the XRD patterns (Salari and Sadeghinia, 2019, Wang et al., 2015a). Sharp diffraction peaks at 2Θ= 38.5 and 60 are related to the (111) and (103) plane of CuO respectively. The peaks at 32, 34.5 and 47.7 are corresponded to (110), (002) and (102) of hexagonal ZnO (PDF# 01-070-303 and PDF#01-075-1533) (Salari and Sadeghinia, 2019).

The FTIR spectra of ZnO/CuO and Zn-Cu-BTC MOF are illustrated in Fig. 2B. The peaks at approximately 480 cm^{-1}, 530 cm^{-1}, and 580 cm^{-1} are related to the vibrations of Cu-O (Azam et al., 2012). The band centered at 436 cm^{-1} attributed to the Zn–O stretching mode of the ZnO lattice. The Zn-Cu-BTC MOF peak below 2000 cm^{-1} had bands of carboxylate group absorption. The presence of weakly bound water molecules on the ZnO/CuO surface and inside the metal organic framework pores is indicated by the wide band detected above 3300 cm^{-1} (Autie-Castro et al., 2015). The C=C and C=O peaks were appeared at 1650 cm^{-1} and 1750 cm^{-1}, respectively.

Using a scanning electron microscope (SEM), the morphology of surface and particle size were examined. As seen in Fig. 2, the size of nanoparticles are smaller than 80 nm which distributed uniformly.

As seen in Fig. 3, the EDX spectrum provided additional evidence for the occurrence of Zn, Cu, and O. Additionally, the EDX elemental mapping photos clearly display the distribution of

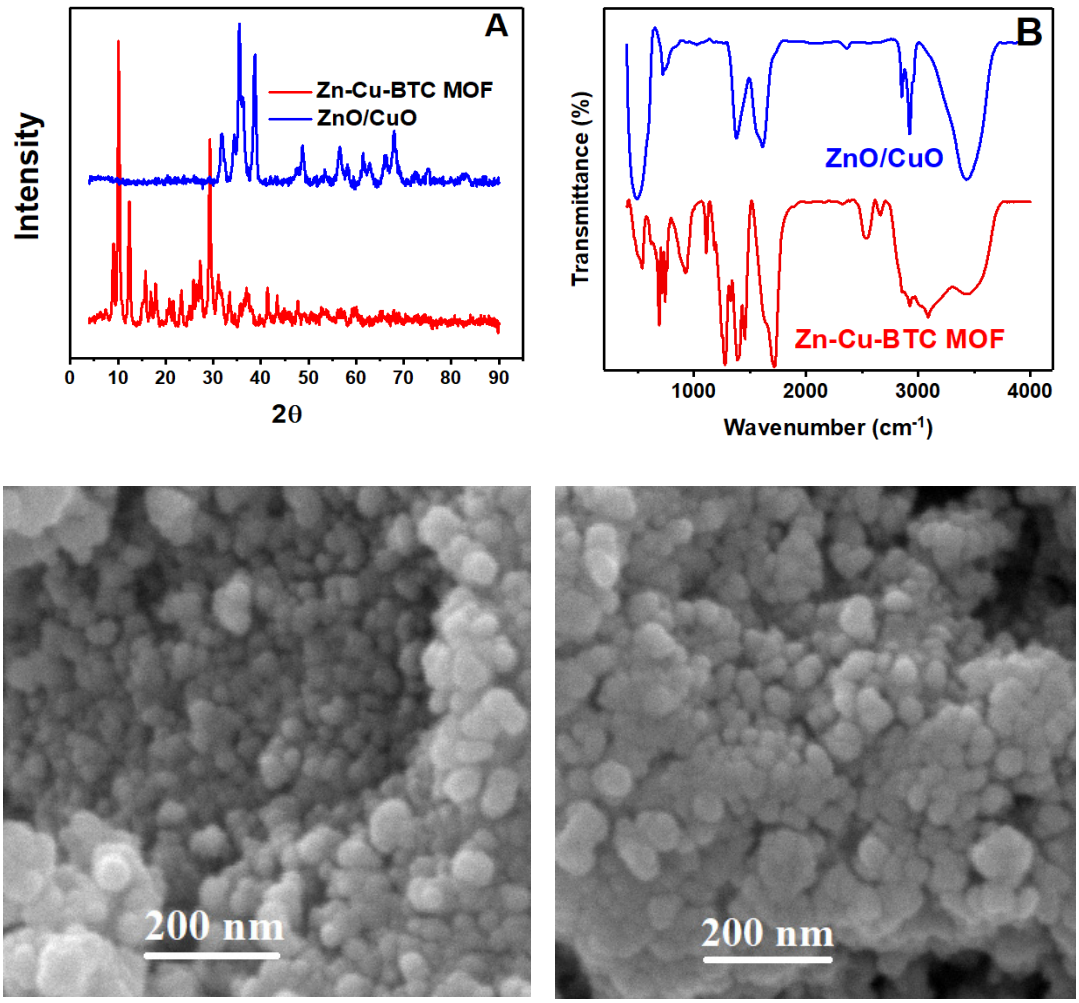

Fig. 2. XRD patterns (A) and FTIR spectra (B) of Cu(50)-Zn(50)-BTC MOF and ZnO/CuO and SEM images of prepared ZnO/CuO (Down-left and Down-right).

the elements Zn, Cu, and O. (Fig. 3). The EDX mapping pictures of ZnO/CuO further show that the distribution of Zn, Cu, and O components inside the nanostructure is uniform.

These outcomes amply demonstrate that ZnO/CuO was produced successfully. The amount of carbon was zero demonstrated that MOF ligand was removed completely during pyrolysis.

X-ray photoelectron spectroscopy technique was applied for elements chemical state investigation. XPS spectrum of ZnO/CuO are exhibited in Fig. 4 and the presence of Zn, O and Cu was detected by scanning of the surface in the range of 0 to 1000 eV. No other elements were detected and it proves the purity of produced material. Detailed surface scans were performed for core level of Cu2p, Zn2p and O1s peaks. As illustrated in Fig. 4, the data points were fitted using Gaussian-Lorentzian fits. After de-convolution of Zn2p peak, two peaks appeared at 1024 and 1043 eV which corresponded to the Zn $2p_{3/2}$ and Zn $2p_{1/2}$ level respectively. These peaks related to Zn ion in a hexagonal wurtzite ZnO structure (Salari and Sadeghinia, 2019, Vuong et al., 2016). The high resolution Cu2p peak revealed two peaks at 935 and 958 eV which corresponded to $2p_{3/2}$ and $2p_{1/2}$.

These peaks approved the presence of CuO structure in composite with the +2 oxidation state of copper (Salari and Sadeghinia, 2019, Vuong et al., 2016). The signal associated to O1s centered at 529.5 eV demonstrates bonding between O_2^- ions and Zn/Cu (Biesinger et al., 2011, Behera and Chandra, 2015). The sub-peak at 532.18 eV is corresponded to O_2^- ions in oxygen-

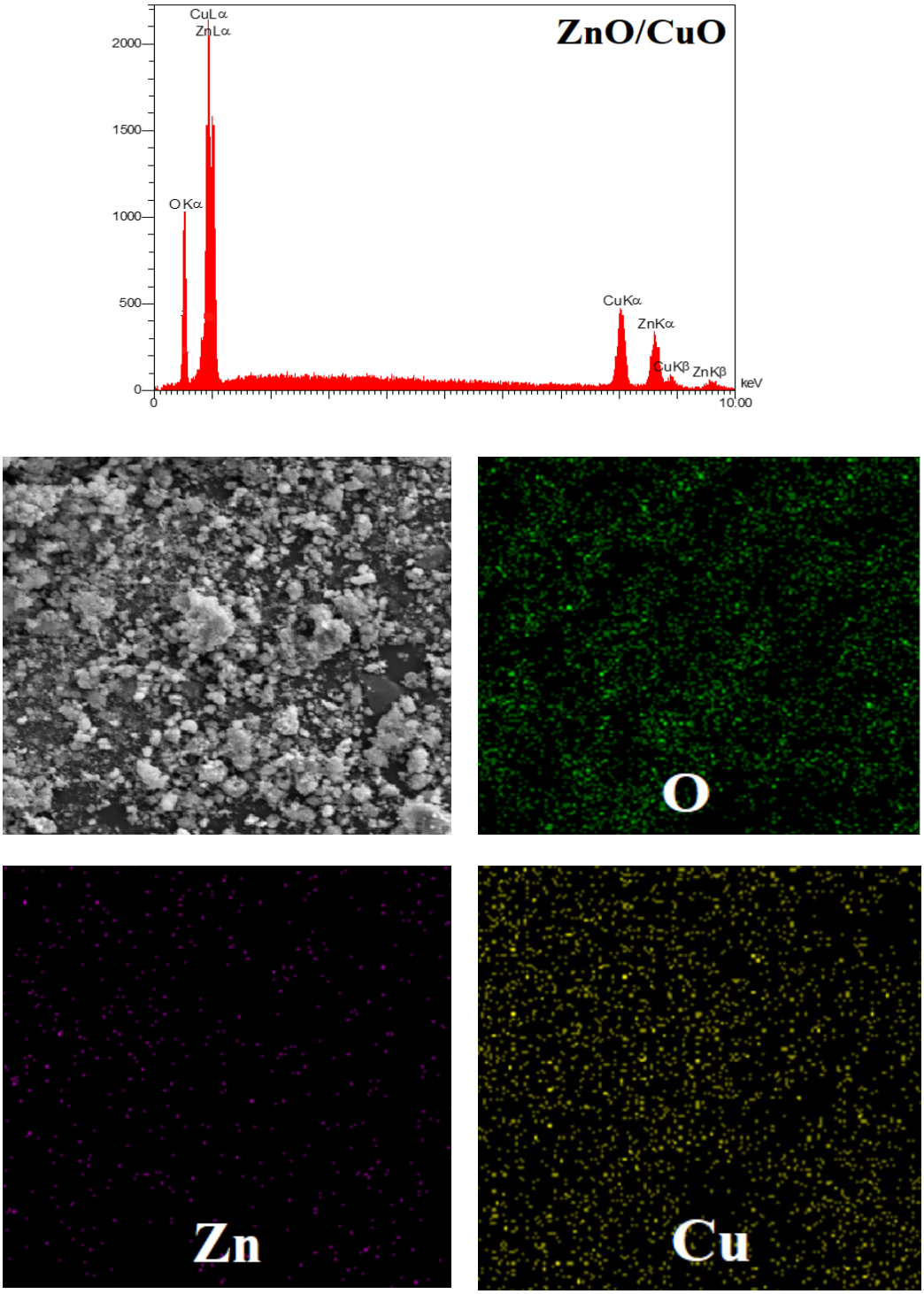

Fig. 3. EDX analysis and EDX mapping of ZnO/CuO.

deficient locations and/or H_2O or O_2 molecule adsorption (Behera and Chandra, 2015).

Optimization strategy

Preliminary experiments

The main factors for chromate removal that were measured while the temperature and stirring rate were held constant at 298 K and 800 rpm, respectively, were sample pH (2-4), hole

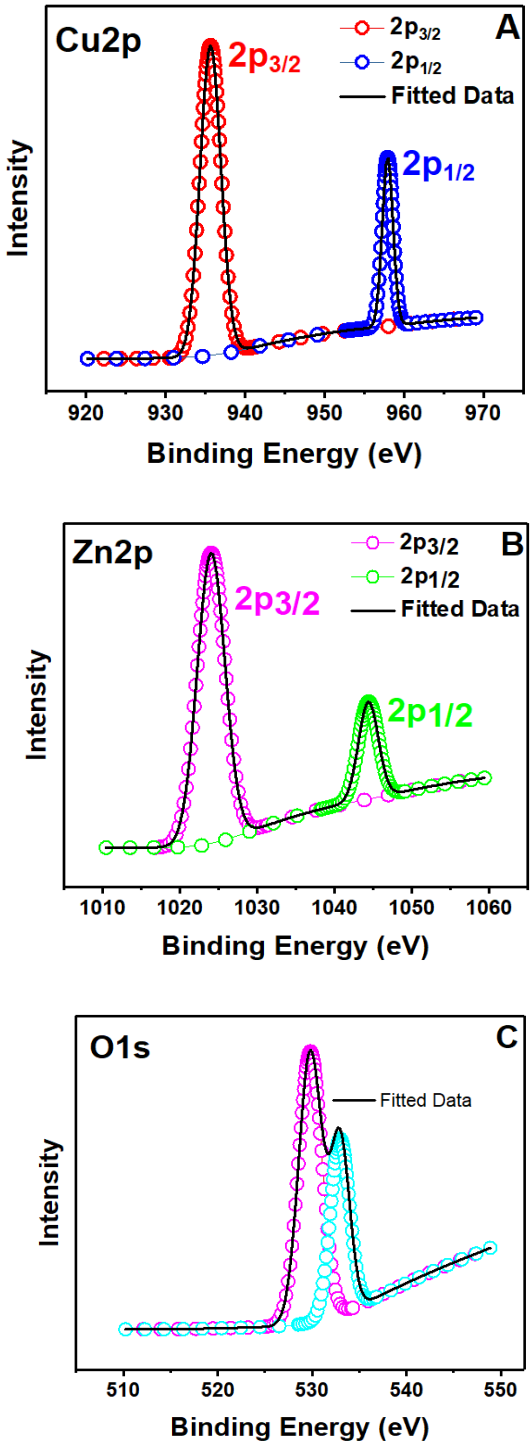

Fig. 4. XPS spectra of ZnO/CuO and high resolution spectrum of Zn, Cu and O.

scavenger type (citric, formic, and oxalic acids), chromate ion concentration (5-200 ppm), ZnO/CuO dosage (10-20 mg), and contact duration (10-20 min).

At the first, the effect of citric acid, formic acid, and oxalic acid as different hole scavenger types were investigated and the results showed O1s is the best (see Fig. 5). Then, the levels of the mentioned factors were selected based on preliminary experiments. The following utilized central composite design (CCD) and the trial version of the Design Expert 10.0.0 package to

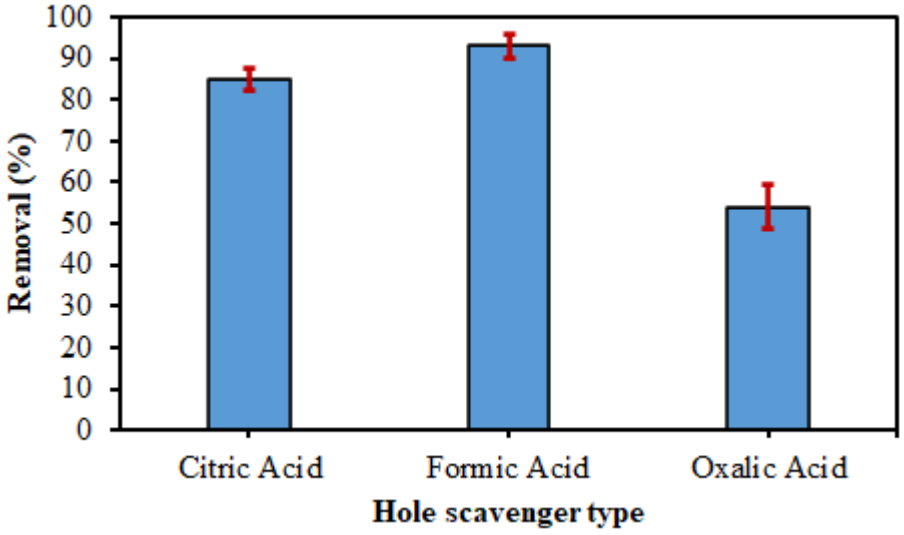

Fig. 5. Effect of hole scavenger type on the chromate removal using the proposed ZnO/CuO as both adsorbent and catalyst.

model and optimize the impact of the other listed effective parameters on the chromate removal efficiency (Stat-Ease Inc., Minneapolis, MN, USA).

Central composite design

The first findings revealed that the aforementioned are the main parameters in the chromate removal process, hence it is necessary to optimize them. In the first step, the removal procedure was performed based on the software proposed CCD matrix, and then the Box–Cox plot was investigated, indicating that the response can be used without any transformation, (Fig. 6). The final result was reported as the average of three determinations, and the variances were calculated using one degree of freedom (DOF). Calculating the standard errors of the effects was the step required for comparing and emphasizing the primary impacts. The analysis of variance (ANOVA) approach was used to determine the main effects' and interactions' significant values (Table 1). The small level of significance (P) state that the main effects and their interaction are statistically significant when P-value < 0.05 for confidence level of 95% (Montgomery, 2017, Moghaddam et al., 2018). The model's respective F-value, which measures its significance, was 84.71, which shows that the likelihood of noise is under 0.01%. P-values under and over 0.0500 denoted the model's relative significance and insignificance. Therefore, the A, B, C, and their quadratic terms were found to be significant. The reduction model may be used to numerous unimportant model variables to enhance the outcomes and prevent over-fitting. Therefore, the following coded equation was obtained for chromate removal using the proposed ZnO/CuO.

$$\text{Removal}(\%) = +88.5 - 11.10A + 4.95B + 3.19C - 3.37A^2 - 2.14B^2 - 2.14C^2 \quad (2)$$

In comparison to the pure error, the "Lack of Fit (LOF) F-value" was determined to be 2.58, which was inconsequential. According on the model's projected and adjusted R^2 values ($R^2_{Pred.}$, $R^2_{Adj.}$), there is very little likelihood that the updated model will contain any minor variables. It is obvious that in these situations, the ZnO/CuO ratio and contact duration have a beneficial impact on the elimination of chromate ions whereas the sample pH has a negative impact. To further validate the improved models, plots of the normal probability of the studentized residuals for chromate removal (Fig. 6) were created. This graphic demonstrates that the residuals have a

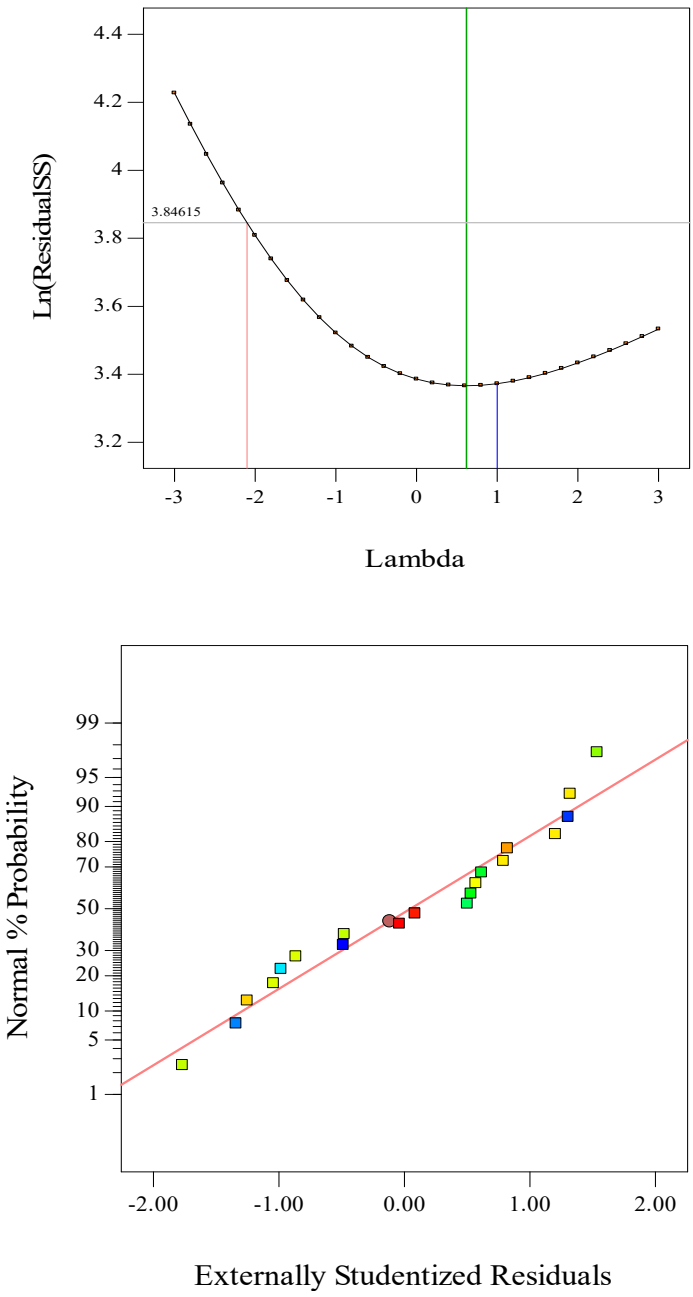

Fig. 6. The Box-Cox plot for chromate removal model using ZnO/CuO (up) and normal probability plot for the proposed model (down).

normal distribution and that the points are on a straight line.

The correlations between the removal efficiency and the degree of each component are displayed in the 3D plots of the models. These plots were created while keeping the other parameters constant by comparing the response values of the models to two additional experimental factors.

Fig. 7 shows the plot of the initial pH versus ZnO/CuO amount (mg); pH versus contact time (min); and ZnO/CuO amount (mg) versus contact time (min), for chromate ions removal.

The model, which makes use of experimental data, produced the best values for the examined variables. The procedure of optimization aimed to increase the effectiveness of chromate ions

Table 1. ANOVA table for chromate removal using ZnO/CuO.

Source	SS[a]	DF[b]	MS[c]	F-value	p-value	
Block	11.49	2	5.75			
Model	2452.57	9	272.51	74.81	< 0.0001	significant
A-pH	1681.63	1	1681.63	461.65	< 0.0001	
B-ZnO/CuO amount	334.52	1	334.52	91.83	< 0.0001	
C-Time	138.56	1	138.56	38.04	0.0003	
AB	3.13	1	3.13	0.86	0.3814	
AC	1.13	1	1.13	0.31	0.5936	
BC	10.13	1	10.13	2.78	0.1340	
A^2	200.33	1	200.33	55.00	< 0.0001	
B^2	65.88	1	65.88	18.09	0.0028	
C^2	65.88	1	65.88	18.09	0.0028	
Residual	29.14	8	3.64			
Lack of Fit	23.64	5	4.73	2.58	0.2327	not significant
Pure Error	5.50	3	1.83			
Cor Total	2493.20	19				
R^2	0.9825					
Adjusted R^2	0.9729					
Predicted R^2	0.9458					

[a] Sum of square (SS)
[b] Degree of freedom (DF)
[c] Mean square (MS)

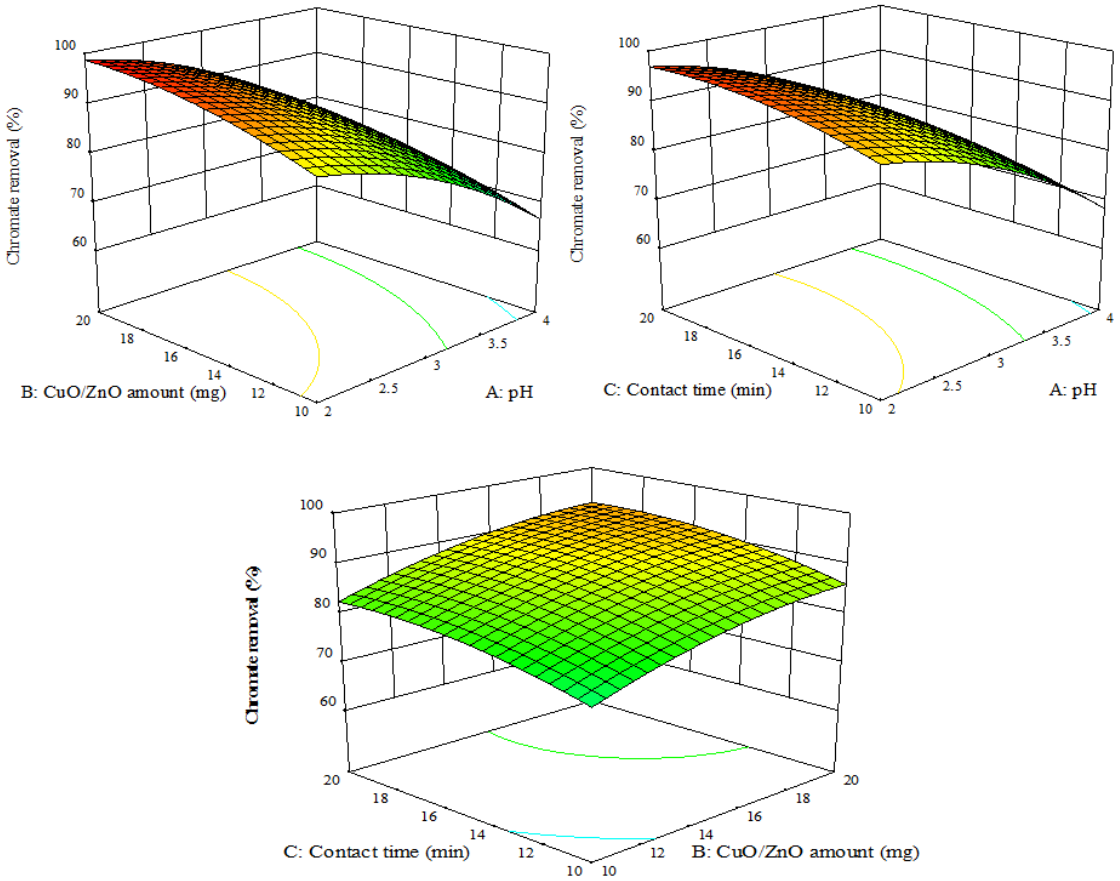

Fig. 7. 3D response surface plots for chromate removal.

removal. For optimization and follow-up on a multi-dimensional uphill downhill simplex (Nelder-Mead) design, Design-Expert 10.0.0 trial version was employed. The non-linear optimization approach produced the findings, defining the pH of 2.0, ZnO/CuO amount of 20.0 mg, and contact time of 17.8 min for removal of chromate ions from solutions containing 50 ppm chromate. The final results of the expected and experimental responses were 99.7±2.0% and 95.0±2.7%.

Mechanism studies for chromate reduction

It seems that the proposed ZnO/CuO had an efficient catalytic performance for converting Cr (VI) to Cr (III). Moreover, the adsorption phenomenon was observed. To confirm Cr (VI) removal mechanism, the amount of total Cr was obtained via Atomic absorption spectrometry to affirm our proposed mechanism.

The reduction ratio can be estimated by considering Cr (III) which can be obtained from the difference of total Cr and Cr (VI) amounts. In addition, ZnO/CuO assisted in the surface adsorption process of Cr (VI) interacting with the functional groups on ZnO/CuO surfaces, and then converting to Cr (III). By FAAS analyzing the treated solution after the reaction, the Cr (III) and remaining Cr (VI) in the treated solution are obvious. As a consequence, after adsorption, Cr (VI) is converted on the surface, and ZnO/CuO reduces Cr (VI) effectively.

Isotherm studies

The well-known Langmuir, Freundlich, and Tempkin isotherm models were used to mimic the experimental results. The chromate ions' adsorption isotherms on ZnO/CuO at 298K are depicted in Fig. 8. Here, the capacity of ZnO/CuO, as indicated by Eq. 3, increases significantly and plateaus. It implies that ZnO/CuO might be saturated at high enough starting chromate ion concentrations. Our findings shown that by increasing the initial chromate ions concentration from 5 to 200 ppm, the capacity at equilibrium rose from 2.5 to 37.3 mg g^{-1}. The mass transfer barrier of the chromate ions from the aqueous to solid phases is overcome due to a rise in the concentration of chromate ions in the aqueous media, making it easier for the ions to move from the bulk solution to the ZnO/CuO surface (Wu et al., 2001).

When the adsorption process adheres to the monolayer adsorption, the experimental data for the adsorption systems might be well-fitted to the linear Langmuir isotherm using the following equation:

$$\frac{C_e}{q_e} = \frac{1}{K_L q_m} + \frac{C_e}{q_m} \tag{3}$$

where q_m is the maximum capacity of ZnO/CuO (mg g^{-1}) and K_L is the Langmuir constant (L mg^{-1}) which is related to the free energy of chromate ions adsorption on ZnO/CuO process.

The highest chromate ion adsorption capacity of the ZnO/CuO was estimated to be 44.8 mg g^{-1} based on Langmuir adsorption isotherms. Additionally, the values of R_L, which were computed using the following equation, were used to assess how suitable ZnO/CuO was for chromate ions:

$$R_L = \frac{1}{1 + K_L C_0} \tag{4}$$

The R_L values between 0 and 1 indicates favorable adsorption. The obtained R_L value of 0.406 indicates favorable adsorption across the investigated concentration ranges.

The well-known logarithmic form of the Freundlich isotherm is given by the following equation (Ren et al., 2013, Li et al., 2012).

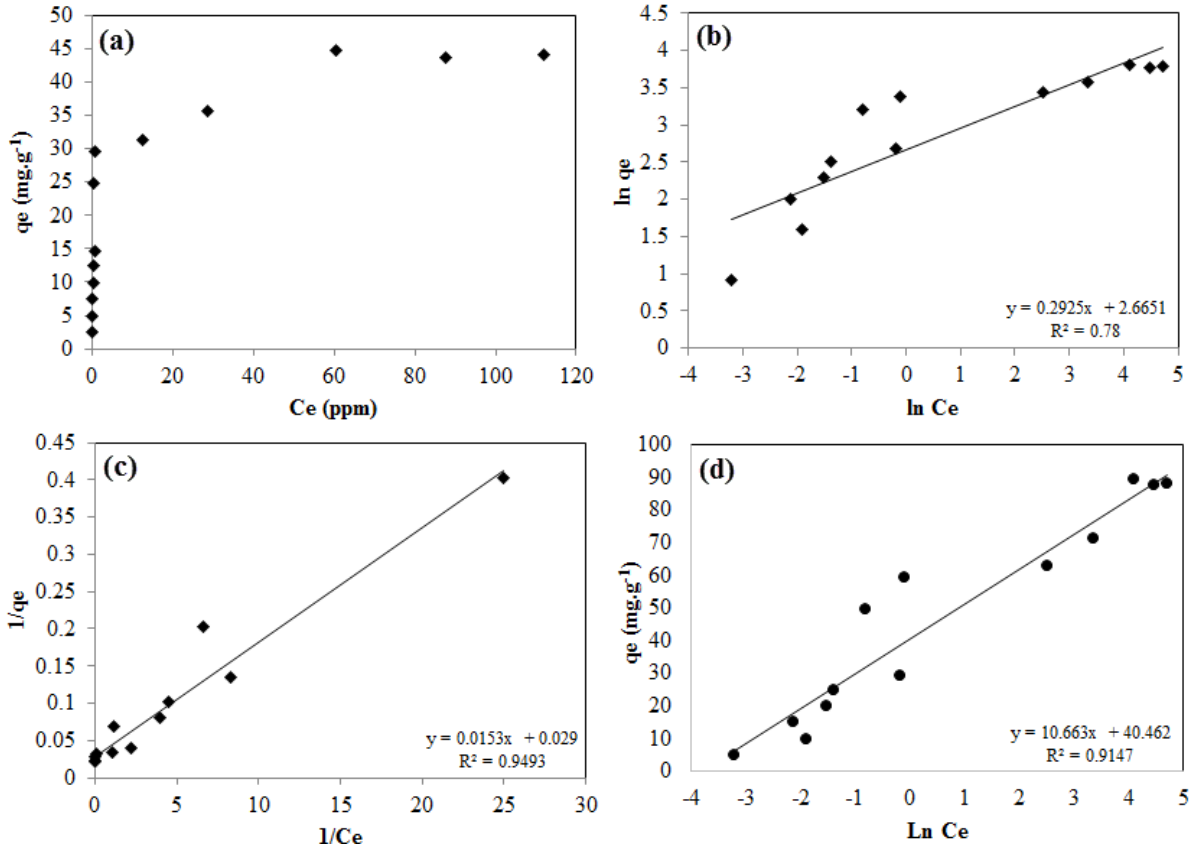

Fig. 8. a) q_e vs C_e, and linear form of the isotherm models of b) Freundlich (ln q_e vs lnC_e), c) Langmuir ($1/q_e$ vs $1/C_e$), and d) Temkin (q_e vs lnC_e).

$$\ln(q_e) = \ln(K_F) + \frac{1}{n}\ln(C_e) \quad (5)$$

K_F (L mg^{-1}) and n are Freundlich constants in this instance. K_F is a function of the adsorbent's capacity for adsorption, and n provides a clue as to how advantageous the adsorption process is. Values of $2 < n < 10$, $1 < n < 2$ and <1 correspondingly display good, challenging, and bad adsorption capabilities. The number n is 3.4 (see Table 2), which indicates that it has high adsorption properties. The adsorption isotherms of chromate ions on the created ZnO/CuO are shown in Fig. 8.

The correlation coefficients from the linearized Langmuir and Freundlich isotherms are presented in Figure 8 and listed in Table 2, showing a better experimental data fitting towards the Langmuir isotherm and indicating that a monolayer of chromate ions has formed on the surface as a result of the process. However, the chromate ions may be removed catalytically following adsorption.

Also, the experimental data were investigated with the Temkin isotherm, which is expressed by Eq. 6, to evaluate the adsorption phenomena.

$$q_e = \frac{RT}{b_T}\mathrm{Ln}(K_{Te}.C_e) \quad (6)$$

Table 2. Langmuir, Freundlich and Temkin parameters for the adsorption of chromate ions on proposed ZnO/CuO.

Langmuir constants				Freundlich constants			Temkin		
q_m (mg g^{-1})	b	R_L	R^2	n	K_f	R^2	b_T (J mol^{-1})	K_T (L g^{-1})	R^2
44.5	0.03	0.406	0.9493	3.4	14.4	0.7800	232.4	42744.7	0.9147

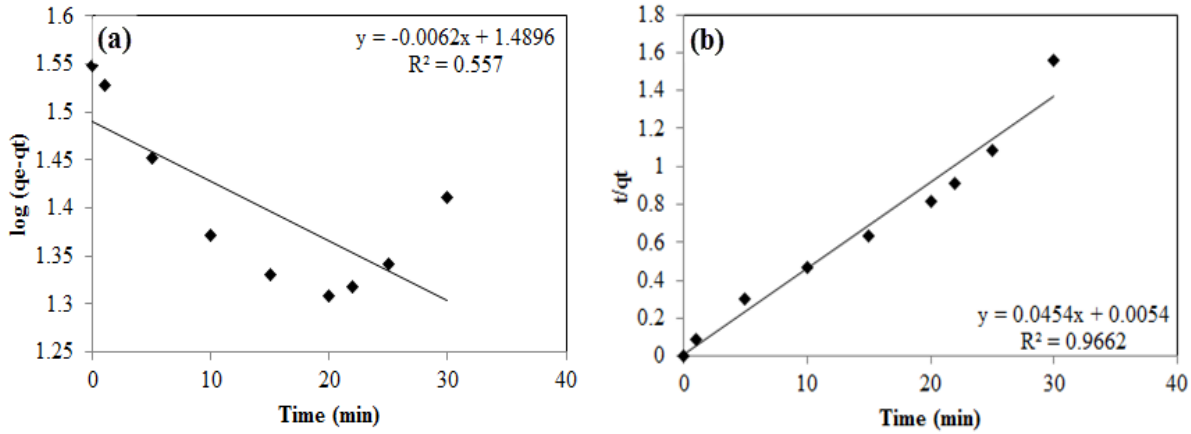

Fig. 9. a) pseudo-first order and b) pseudo-second order kinetic models for removal of chromate ions using proposed ZnO/CuO.

The linear form of the isotherm is given by the following Eq.:

$$q_e = A + BLnC_e \quad (7)$$

$$A = \left(\frac{RT}{b_T} LnK_{Te}\right) \quad (8)$$

$$B = \left(\frac{RT}{b_T}\right) \quad (9)$$

A and B are model constants, K_{Te} is the equilibrium binding constant (L/g), R is the gas constant (8.341 J mol^{-1} K^{-1}), T is the absolute temperature (K), and b_T is a function of the heat of adsorption (J mol^{-1}). According to the correlation coefficient, the Temkin model is also capable of predicting the equilibrium conditions for the adsorption and chemisorption of chromate ions on the ZnO/CuO surface.

Kinetic studies

On the ZnO/CuO, the chromate ions' adsorption kinetic parameters were calculated. To fit the experimental results, kinetic models, including pseudo-first-order and pseudo-second-order, were used (see Fig. 9). Table 3 lists the calculated outcomes of these fits. The pseudo-first order kinetic model was the Lagergren equation, which was based on solid capacity (Sepehr et al., 2013, Tanhaei et al., 2015, Zeraatkar Moghaddam et al., 2019).

$$\ln\left(q_e - q_t\right) = \ln q_e - k_1 t \quad (10)$$

Table 3. Kinetic parameters for the removal of chromate ions using the proposed ZnO/CuO.

Time (min)	C_o (ppm)	Pseudo-first-order			Pseudo-second-order		
		q_e (mg g^{-1})	k_1 (min^{-1})	R^2	q_e (mg g^{-1})	k_2 (min^{-1})	R^2
0-30	50	30.9	0.0143	0.5570	22.0	0.0054	0.9662

Table 4. Comparing various adsorbents containing for chromate removal from aqueous solution.

Materials	pH	Catalyst dose (mg.L^{-1})	Chromate conc. (ppm)	Time (min)	Ref.
Magnetic nanoscale zerovalent iron assisted biochar	6.0	2000	50	1440	*(Zhu et al., 2017)*
Nanoscale zerovalent iron particles supported on herb-residue biochar	2.0	200	20	30	*(Shang et al., 2017)*
Raw biochar and modified biochars supported zero valent iron nanopartilces	5.0	200	10	120	*(Dong et al., 2017)*
Silicon-rich biochar-supported nanoscale zero-valent iron	3.0	200	50	1440	*(Qian et al., 2019)*
Metal oxide nanocomposite derived from bimetallic metal organic framework	2.0	2000	50	17.8	*This work*

Hence the slope of the linear plot of ln (q_e-q_t) *vs* time may be used to derive the value of the pseudo-first order rate constant k_1.

Equation (11) is the linear version of the pseudo-second order kinetic model, and it was also used to test the experimental results (Zeraatkar Moghaddam et al., 2019).

$$\frac{t}{q_t} = \frac{1}{k_2 q_e^2} + \frac{t}{q_e} \tag{11}$$

where the second-order rate constant is k_2 (g mg^{-1} min^{-1}). A straight line with a slope of $1/q_e$ and an intercept of $1=k_2q_e^2$ results from the plot of t/q_t versus t (Fig. 9).

The supplied function specifies the quantity of chromate ions removed at equilibrium ($q_{e,cal}$) as well as the rate constant (k_2). Table 3's regression coefficient values for pseudo-first and second order kinetic models amply demonstrate that the pseudo-second order model was successful in describing the chromate elimination process.

According to presented comparison table (see Table 4), various factors, such as sample pH, contact time, nanomaterials dose, and initial concentration of chromate, were compared with other reported hybrid materials. The results showed that the proposed ZnO/CuO nanao-material had shown high efficiency of over 95% at lower times among the other hybrid materials.

CONCLUSIONS

In conclusion, we showed a novel method for producing high surface area hybrid metal oxide nanocomposite from bimetallic MOF. Chromate ions were researched as a sample contaminant,

and the creation and use of a new low-cost, environmentally friendly material made of ZnO/CuO serving as both an adsorbent and catalyst concurrently was studied. This harmful anion may be removed from the water sample effectively using the suggested ZnO/CuO from MOF. The simplex non-linear optimization was used to improve the procedure settings to enhance the removal efficiency of chromate ions. The chromate ions removal model was extremely well in agreement with the experimental results, as seen by the corrected and anticipated correlation coefficients. The non-linear optimization approach produced the findings, defining the pH of 2.0, catalyst amount of 20.0 mg, and contact time of 17.8 minutes for chromate removal from solutions containing 50 ppm chromate.

In less than 20 minutes, the operation achieved the equilibrium state. The Langmuir and Temkin models were discovered to follow the best-fit chromate ions adsorption isotherms, representing the homogeneity and chemisorption of the adsorption phenomena. According to kinetic studies, the chromate ions adhere to a pseudo-second-order kinetic model when they interact with the ZnO/CuO.

ACKNOWLEDGMENT

We would like to thank Research Council, Shiraz University and University of Birjand for the financial support.

CONFLICT OF INTEREST

The authors declare that there is not any conflict of interests regarding the publication of this manuscript. In addition, the ethical issues, including plagiarism, informed consent, misconduct, data fabrication and/ or falsification, double publication and/or submission, and redundancy has been completely observed by the authors.

LIFE SCIENCE REPORTING

No life science threat was practiced in this research.

REFERENCES

Ajmal, M., Nomani, A. A., & Ahmad, A. (1984) Acute toxicity of chrome electroplating wastes to microorganisms: adsorption of chromate and chromium (VI) on a mixture of clay and sand. *Water, Air, and Soil Pollution,* **23,** 119-127.

Autie-Castro, G., Autie, M., Rodríguez-Castellón, E., Aguirre, C., & Reguera, E. (2015) Cu-BTC and Fe-BTC metal-organic frameworks: Role of the materials structural features on their performance for volatile hydrocarbons separation. *Colloids and Surfaces A: Physicochemical and Engineering Aspects,* **481,** 351-357.

Azam, A., Ahmed, A. S., Oves, M., Khan, M., & Memic, A. (2012) Size-dependent antimicrobial properties of CuO nanoparticles against Gram-positive and-negative bacterial strains. *International journal of nanomedicine***,** 3527-3535.

Babiker, I. S., Mohamed, M. A., Terao, H., Kato, K., & Ohta, K. (2004) Assessment of groundwater contamination by nitrate leaching from intensive vegetable cultivation using geographical information system. *Environment International,* **29** (8)**,** 1009-1017.

Barlik, N., Keskinler, B., & Kocakerim, M. M. (2016) Hexavalent chromium removal performance of anionic functionalized monolithic polymers: column adsorption, regeneration and modelling. *Water Science and Technology,* **73** (6)**,** 1279-1286.

Behera, B., & Chandra, S. (2015) Synthesis and characterization of ZnO nanowires and ZnO–CuO nanoflakes from sputter-deposited brass (Cu0. 65–Zn0. 35) film and their application in gas sensing. *Journal of Materials Science & Technology,* **31** (11)**,** 1069-1078.

Biesinger, M. C., Payne, B. P., Grosvenor, A. P., Lau, L. W., Gerson, A. R., & Smart, R. S. C. (2011)

Resolving surface chemical states in XPS analysis of first row transition metals, oxides and hydroxides: Cr, Mn, Fe, Co and Ni. *Applied Surface Science,* **257** (7)**,** 2717-2730.

Dong, H., Deng, J., Xie, Y., Zhang, C., Jiang, Z., Cheng, Y., Hou, K., & Zeng, G. (2017) Stabilization of nanoscale zero-valent iron (nZVI) with modified biochar for Cr (VI) removal from aqueous solution. *Journal of Hazardous Materials,* **332,** 79-86.

Feldblyum, J. I., Liu, M., Gidley, D. W., & Matzger, A. J. (2011) Reconciling the discrepancies between crystallographic porosity and guest access as exemplified by Zn-HKUST-1. *Journal of the American Chemical Society,* **133** (45)**,** 18257-18263.

Furukawa, H., Cordova, K. E., O'Keeffe, M., & Yaghi, O. M. (2013) The chemistry and applications of metal-organic frameworks. *Science,* **341** (6149)**,** 1230444.

Gao, Q., Xu, J., & Bu, X.-H. (2019) Recent advances about metal–organic frameworks in the removal of pollutants from wastewater. *Coordination Chemistry Reviews,* **378,** 17-31.

Golbaz, S., Jafari, A. J., Rafiee, M., & Kalantary, R. R. (2014) Separate and simultaneous removal of phenol, chromium, and cyanide from aqueous solution by coagulation/precipitation: Mechanisms and theory. *Chemical Engineering Journal,* **253,** 251-257.

Li, C., Chen, T., Xu, W., Lou, X., Pan, L., Chen, Q., & Hu, B. (2015) Mesoporous nanostructured Co_3O_4 derived from MOF template: a high-performance anode material for lithium-ion batteries. *Journal of Materials Chemistry A,* **3** (10)**,** 5585-5591.

Li, J., Jin, R., Liu, G., Tian, T., Wang, J., & Zhou, J. (2016) Simultaneous removal of chromate and nitrate in a packed-bed bioreactor using biodegradable meal box as carbon source and biofilm carriers. *Bioresource technology,* **207,** 308-314.

Li, Y., Sui, K., Liu, R., Zhao, X., Zhang, Y., Liang, H., & Xia, Y. (2012) Removal of methyl orange from aqueous solution by calcium alginate/multi-walled carbon nanotubes composite fibers. *Energy Procedia,* **16,** 863-868.

Liu, J., He, X.-x., Lin, X.-r., Chen, W.-c., Zhou, Q.-x., Shu, W.-s., & Huang, L.-n. (2015) Ecological effects of combined pollution associated with e-waste recycling on the composition and diversity of soil microbial communities. *Environmental science & technology,* **49** (11)**,** 6438-6447.

Moghaddam, A. Z., Ghiamati, E., Pourashuri, A., & Allahresani, A. (2018) Modified nickel ferrite nanocomposite/functionalized chitosan as a novel adsorbent for the removal of acidic dyes. *International journal of biological macromolecules,* **120,** 1714-1725.

Montgomery, D. C. (2017) *Design and analysis of experiments*. John wiley & sons.

Nalbandian, M. J., Zhang, M., Sanchez, J., Choa, Y.-H., Nam, J., Cwiertny, D. M., & Myung, N. V. (2016) Synthesis and optimization of Fe2O3 nanofibers for chromate adsorption from contaminated water sources. *Chemosphere,* **144,** 975-981.

Olivares, A., Quirós, L., Pelayo, S., Navarro, A., Bosch, C., Grimalt, J. O., del Carme Fabregat, M., Faria, M., Benejam, L., & Benito, J. (2010) Integrated biological and chemical analysis of organochlorine compound pollution and of its biological effects in a riverine system downstream the discharge point. *Science of the total environment,* **408** (22)**,** 5592-5599.

Qian, L., Shang, X., Zhang, B., Zhang, W., Su, A., Chen, Y., Ouyang, D., Han, L., Yan, J., & Chen, M. (2019) Enhanced removal of Cr (VI) by silicon rich biochar-supported nanoscale zero-valent iron. *Chemosphere,* **215,** 739-745.

Ren, Y., Abbood, H. A., He, F., Peng, H., & Huang, K. (2013) Magnetic EDTA-modified chitosan/SiO_2/Fe_3O_4 adsorbent: preparation, characterization, and application in heavy metal adsorption. *Chemical Engineering Journal,* **226,** 300-311.

Saha, R., Nandi, R., & Saha, B. (2011) Sources and toxicity of hexavalent chromium. *Journal of Coordination Chemistry,* **64** (10)**,** 1782-1806.

Salari, H., Erami, M., Dokoohaki, M. H., & Zolghadr, A. R. (2022) New insights into adsorption equilibrium of organic pollutant on MnO_2 nanorods: Experimental and computational studies. *Journal of Molecular Liquids,* **345,** 117016.

Salari, H., & Sadeghinia, M. (2019) MOF-templated synthesis of nano Ag_2O/ZnO/CuO heterostructure for photocatalysis. *Journal of Photochemistry and Photobiology A: Chemistry,* **376,** 279-287.

Salari, H., & Zahiri, Z. (2022) Design of S-scheme 3D nickel molybdate/AgBr nanocomposites: Tuning of the electronic band structure towards efficient interfacial photoinduced charge separation and remarkable photocatalytic activity. *Journal of Photochemistry and Photobiology A: Chemistry,* **426,** 113751.

Sepehr, M. N., Sivasankar, V., Zarrabi, M., & Kumar, M. S. (2013) Surface modification of pumice

enhancing its fluoride adsorption capacity: An insight into kinetic and thermodynamic studies. *Chemical Engineering Journal,* **228,** 192-204.

Shaislamov, U., Krishnamoorthy, K., Kim, S. J., Abidov, A., Allabergenov, B., Kim, S., Choi, S., Suresh, R., Ahmed, W. M., & Lee, H.-J. (2016) Highly stable hierarchical p-CuO/ZnO nanorod/nanobranch photoelectrode for efficient solar energy conversion. *international journal of hydrogen energy,* **41** (4)**,** 2253-2262.

Shamshirgaran, R., Malakooti, R., Akbarpour, A., & Moghaddam, A. Z. (2022) Fabrication of Polyvinylpyrrolidone-Stabilized Nano Zero-Valent Iron Supported by Hydrophilic Biochar for Efficient Cr (VI) Removal from Groundwater. *ChemistrySelect,* **7** (43)**,** e202202927.

Shang, J., Zong, M., Yu, Y., Kong, X., Du, Q., & Liao, Q. (2017) Removal of chromium (VI) from water using nanoscale zerovalent iron particles supported on herb-residue biochar. *Journal of Environmental Management,* **197,** 331-337.

Shao, J., Wan, Z., Liu, H., Zheng, H., Gao, T., Shen, M., Qu, Q., & Zheng, H. (2014) Metal organic frameworks-derived Fe_3O_4 hollow dodecahedrons with controllable interiors as outstanding anodes for Li storage. *Journal of Materials Chemistry A,* **2** (31)**,** 12194-12200.

Sharma, S. K., Petrusevski, B., & Amy, G. (2008) Chromium removal from water: a review. *Journal of Water Supply: Research and Technology—AQUA,* **57** (8)**,** 541-553.

Shayeh, J. S., & Salari, H. (2020) Dendritic fibrous nano metal organic framework: A magnetic core-shell structure as high performance material for electrochemical capacitors. *Journal of Energy Storage,* **32,** 101734.

Sołek-Podwika, K., Ciarkowska, K., & Kaleta, D. (2016) Assessment of the risk of pollution by sulfur compounds and heavy metals in soils located in the proximity of a disused for 20 years sulfur mine (SE Poland). *Journal of Environmental Management,* **180,** 450-458.

Tanhaei, B., Ayati, A., Lahtinen, M., & Sillanpää, M. (2015) Preparation and characterization of a novel chitosan/Al_2O_3/magnetite nanoparticles composite adsorbent for kinetic, thermodynamic and isotherm studies of Methyl Orange adsorption. *Chemical Engineering Journal,* **259,** 1-10.

Tzou, Y., Chen, Y., & Wang, M. (1998) Chromate sorption by acidic and alkaline soils. *Journal of Environmental Science & Health Part A,* **33** (8)**,** 1607-1630.

Venkatesh, R., Sekaran, P. R., Udayakumar, K., Jagadeesh, D., Raju, K., & Bayu, M. B. (2022) Adsorption and photocatalytic degradation properties of bimetallic Ag/MgO/biochar nanocomposites. *Adsorption Science & Technology,* **2022**.

Vuong, N. M., Chinh, N. D., & Lee, Y.-I. (2016) CuO-decorated ZnO hierarchical nanostructures as efficient and established sensing materials for H2S gas sensors. *Scientific reports,* **6** (1)**,** 1-13.

Wang, T., Li, X., Dai, W., Fang, Y., & Huang, H. (2015a) Enhanced adsorption of dibenzothiophene with zinc/copper-based metal–organic frameworks. *Journal of Materials Chemistry A,* **3** (42)**,** 21044-21050.

Wang, Z., Liu, Y., Gao, C., Jiang, H., & Zhang, J. (2015b) A porous $Co(OH)_2$ material derived from a MOF template and its superior energy storage performance for supercapacitors. *Journal of Materials Chemistry A,* **3** (41)**,** 20658-20663.

Wielinga, B., Mizuba, M. M., Hansel, C. M., & Fendorf, S. (2001) Iron promoted reduction of chromate by dissimilatory iron-reducing bacteria. *Environmental science & technology,* **35** (3)**,** 522-527.

Wu, F.-C., Tseng, R.-L., & Juang, R.-S. (2001) Kinetic modeling of liquid-phase adsorption of reactive dyes and metal ions on chitosan. *Water research,* **35** (3)**,** 613-618.

Xu, X., Cao, R., Jeong, S., & Cho, J. (2012) Spindle-like mesoporous α-Fe_2O_3 anode material prepared from MOF template for high-rate lithium batteries. *Nano letters,* **12** (9)**,** 4988-4991.

Zeraatkar Moghaddam, A., Ghiamati, E., Ayati, A., & Ganjali, M. (2019) Application of the response surface methodology for optimizing the adsorptive removal of chromate using a magnetic crosslinked chitosan nanocomposite. *Journal of Applied Polymer Science,* **136** (8)**,** 47077.

Zhu, S., Ho, S.-H., Huang, X., Wang, D., Yang, F., Wang, L., Wang, C., Cao, X., & Ma, F. (2017) Magnetic nanoscale zerovalent iron assisted biochar: interfacial chemical behaviors and heavy metals remediation performance. *ACS Sustainable Chemistry & Engineering,* **5** (11)**,** 9673-9682.